RESEARCH ARTICLE

Enhancing Accuracy in Actigraphic Measurements: A Lightweight Calibration Method for Triaxial Accelerometers

DENES FARAGO, BALINT MACZAK, AND ZOLTAN GINGL

Department of Technical Informatics, University of Szeged, 6720 Szeged, Hungary

Corresponding author: Balint Maczak (maczak@inf.u-szeged.hu)

ABSTRACT This paper presents a simple, lightweight, automatic calibration method for low-cost triaxial accelerometers, utilizing the Earth's gravitational constant in various orientations. It can be easily implemented using only fixed-point arithmetic and can run on low-power microcontrollers for real-time measurements, making it practical for scenarios with limited data storage and computational power, such as actigraphy or IoT applications. The method offers ease of use by automatically detecting motionless intervals, eliminating the need for complex positioning techniques. The procedure detects resting states and calculates the corresponding three-dimensional mean acceleration values during the measurement. After appropriately selecting these mean values, a set of calibration points is formed and passed to a gradient-based optimization algorithm for iterative estimation of the calibration coefficients. Different metrics were used for verification and comparison with other methods, which were calculated through simulations and tests based on real measurements. The results show that, despite its lightweight nature, the method performs equally to more complex solutions. This article provides a thorough explanation of a novel method for collecting calibration points, the optimization algorithm, and the methods used for performance evaluation in a reproducible manner.

INDEX TERMS Actigraphy, activity measurement, auto-calibration, calibration, field calibration, MEMS, motion sensors, multi-position calibration, odometry, triaxial accelerometer.

I. INTRODUCTION

The accelerometer has become one of the most widely utilized sensors in the last two decades. There are numerous applications for accelerometers that vary in their sensitivity to the lack of calibration.

The associate editor coordinating the review of this manuscript and approving it for publication was Liang-Bi Chen.

Accelerometers play a crucial role in indoor position tracking within navigation systems, particularly when the GPS signal is unavailable. To achieve indoor tracking after losing the GPS signal, accelerometers are employed to estimate velocity by integrating their output. Subsequently, the position is approximated by integrating the velocity. During these integration processes, errors arising from accelerometer inaccuracies tend to increase quadratically over time, as explained by Titterton and Weston [1]. Ensuring

accurate measurements allows for mitigating the adverse effects of error accumulation and maintaining the integrity of the derived velocity and position estimates.

Accelerometers are extensively employed in various medical applications. They are utilised to monitor human movement for controlling heart rate in pacemakers [2], replicating the motions of a surgeon's hand during robotic-assisted surgery [3], and providing feedback on the quality of chest compressions during CPR [4].

Numerous medical, biological, biophysical, psychological, and sports science research is based on activity measurement, for which wearable activity meters, known as actigraphs, are commonly used devices [5], [6], [7], [8], [9]. Actigraphs are used for measuring human or animal motion, typically incorporating a triaxial accelerometer. The actigraph device operates through a microcontroller that is primarily responsible for facilitating communication between the sensor, flash memory, and PC software, enabling the transmission of recorded activity data. To ensure minimal disruption to an individual's movements, especially during prolonged use over several weeks, actigraphs are designed to be compact in size, similar to a wristwatch. However, this miniaturization limits the battery size and the computation power.

Our research group studies human movement patterns by analysing activity calculated from raw acceleration data which is measured by actigraphs. During our studies, we have acquired numerous datasets containing several weeks of human movement. Many methods have been developed to calculate time-dependent human activity from the raw accelerometer data [10]. Some of these activity metrics are sensitive to the lack of calibration, for example, the Proportional Integration Method requires precise acceleration values since it is based on integration and faces the same problem as the previously mentioned indoor position tracking. Another example of activity calculation that can be affected by offset errors is the Zero Crossing Method, where the number of times the magnitude of acceleration crosses a predetermined threshold level is counted within a specified time interval (epoch). Errors of a poorly calibrated device introduce varying, orientation-dependent biases in the calculated magnitude of acceleration.

Today, due to advances in microelectromechanical systems (MEMS) technology, miniature, reliable, and accurate accelerometers can be produced relatively cheaply. Like in any manufacturing process, devices that are produced have manufacturing imperfections that lead to measurement errors. The extent of these errors may be reduced in a factory through calibration [11], [12]. The provided accuracy is sufficient in most applications; however, it can be improved by further calibration.

According to the datasheet of the LIS3DH sensor used in our activity measurements, the sensor typically has an offset accuracy of ± 40 mg after factory calibration, as shown in Figure 1. In the left figure, the four distinct time intervals measure the local gravity at rest, and therefore the measured

magnitude of acceleration should be the same in each motionless segment. The right figure displays the calibrated version, which shows significant improvement.

The factors affecting measurement errors depend on temperature and battery condition, and may even change between two power-ups of the sensor, therefore, depending on time [13], [14], [15], [16]. Consequently, during long measurements, repetitive re-calibrations may improve the quality of the acquired acceleration data.

Triaxial accelerometer calibration methods may be divided into two groups, depending on whether the calibration is carried out under laboratory conditions by applying precise forces of known accelerations of known directions [14], [17], [18], [19], [20] or using only gravity [21], [22], [23], [24], [25], [26], [27]. The former can be referred to as traditional calibration, while the latter is called multi-position, auto-calibration or field calibration. The advantage of traditional methods is that a known force of any direction and magnitude can be applied to the accelerometer, allowing each axis to be calibrated over its entire range. The drawback of these methods is that the process is time-consuming and requires expensive equipment compared to the cost of the MEMS sensor itself. Gravity-based calibration methods, however, do not require dedicated laboratory instrumentation; only a few measurements of stationary intervals with different angles are necessary.

To keep the actigraph (or any battery-operated IoT device) small, the battery must also be small, which means that the device must be as energy efficient as possible if it is to be used for several days or weeks-long continuous measurements. To record long activity measurements without external power sources, a calibration algorithm for real-time measurements must be simple and CPU efficient to minimize battery usage. For these reasons, we developed a simple procedure with modest computation requirements, but it provides the same level of accuracy as other published methods.

II. METHODS
A. ERROR MODEL
As with every calibration method, ours also involves approximating the errors of the instrument using a mathematical model. Numerous published models exist to describe accelerometer errors, and our implementation relies on a 9-parameter model, which includes the deterministic scale, non-orthogonality, and offset errors. The model is widely used [22], [23], [28], [29], [30], [31] and is well described in [26]. The relationship between the actual and measured quantities can be expressed as follows:

$$\boldsymbol{A} = \boldsymbol{S} \cdot \boldsymbol{T} \left(\boldsymbol{V} + \boldsymbol{O}\right) \qquad (1)$$
$$= \boldsymbol{K} \cdot \left(\boldsymbol{V} + \boldsymbol{O}\right), \qquad (2)$$

where $\boldsymbol{A} = \begin{bmatrix} a_x & a_y & a_z \end{bmatrix}^T$ is the actual triaxial acceleration, $\boldsymbol{V} = \begin{bmatrix} v_x & v_y & v_z \end{bmatrix}^T$ is the measured acceleration subjected to
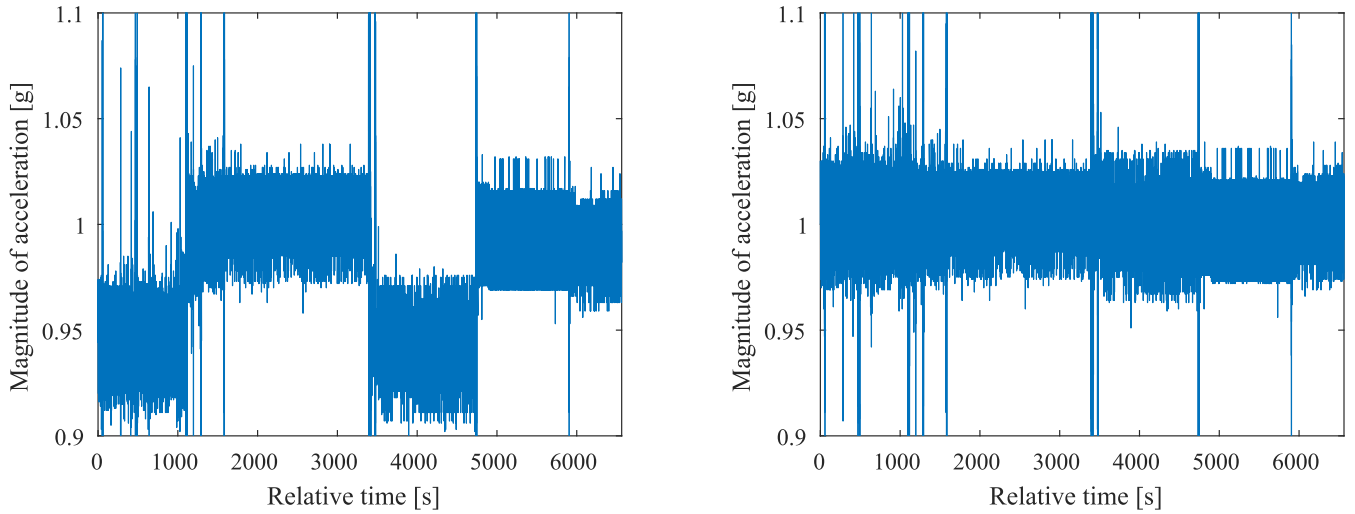
FIGURE 1. The magnitude of acceleration measured by a wrist-worn actigraph during sleep. The plot on the left shows the uncalibrated case, where the device measures 1 g with varying errors across different sleep positions. The plot on the right shows the calibrated version of the same signal.

errors, S is the sensitivity matrix:

$$S = \begin{bmatrix} S_x & 0 & 0 \\ 0 & S_y & 0 \\ 0 & 0 & S_z \end{bmatrix}. \tag{3}$$

T contains the factors for reducing crosstalk between axes, arising due to the non-orthogonality of the three accelerometers:

$$T = \begin{bmatrix} 1 & 0 & 0 \\ T_{xy} & 1 & 0 \\ T_{xz} & T_{yz} & 1 \end{bmatrix} \tag{4}$$

and O is a vector which contains the offset values:

$$O = \begin{bmatrix} O_x & O_y & O_z \end{bmatrix}^T. \tag{5}$$

Ideally, measuring only the gravitational acceleration in g should always yield three-dimensional points that lie on the surface of a unit sphere centered at the origin. However, the 9-parameter model assumes that measuring the gravitational acceleration with an uncalibrated sensor results in points that are on the surface of an ellipsoid instead of a sphere. After obtaining the calibration parameters, this ellipsoid can be transformed into a shape that is closer to a sphere which corresponds to the ideal accelerometer (Figure 2).

The implemented calibration method estimates the elements of K and O:

$$p = \begin{bmatrix} k_{xx} \\ k_{yy} \\ k_{zz} \\ k_{xy} \\ k_{xz} \\ k_{yz} \\ o_x \\ o_y \\ o_z \end{bmatrix}. \tag{6}$$
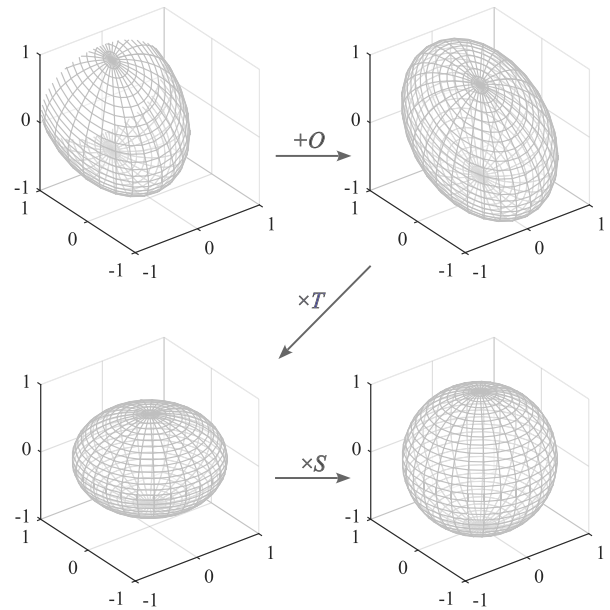

FIGURE 2. Measuring the gravitational acceleration with an uncalibrated sensor results in points on the surface of an ellipsoid instead of a unit sphere. By applying the calibration parameters, the ellipsoid can be shaped closer to a unit sphere that corresponds to an ideal accelerometer. The deviation from the unit sphere in this figure is highly exaggerated to visualize the effect of each calibration parameter.

Given these nine parameters, the acceleration values can be corrected as follows.

$$a_x = k_{xx} (v_x + o_x) \tag{7}$$

$$a_y = k_{xy} (v_x + o_x) + k_{yy} (v_y + o_y) \tag{8}$$

$$a_z = k_{xz} (v_x + o_x)$$
$$+ k_{yz} (v_y + o_y) + k_{zz} (v_z + o_z) \tag{9}$$

B. CALIBRATION PROCEDURE

The calibration procedure consists of two steps. The first involves collecting calibration points, while the second step

estimates the nine parameters of the error model using these points. Calibration at periodic, regular intervals is necessary, as sources of errors may change over time, as is the case with any instrument. The simplified process is depicted in Figure 3.
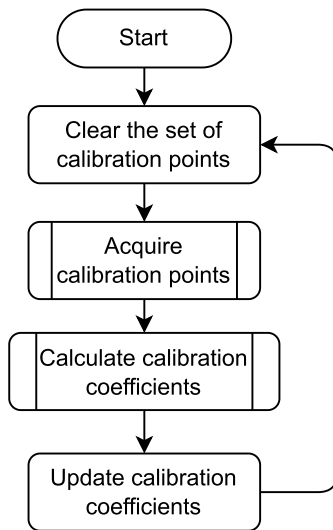

FIGURE 3. The process of calibration involves two main steps: the collection of the calibration points and the estimation of the nine parameters of the error model.

1) ACQUIRING CALIBRATION POINTS

To determine the nine unknowns, it is necessary to gather a minimum of nine distinct and varied averaged three-dimensional acceleration vectors. These calibration points are measured during periods of rest.

The collection process also consists of two steps: First, assessing whether the acceleration during the current time period remains constant or undergoes changes. If constancy is observed, the average value of the obtained three-dimensional acceleration is checked to determine if it differs from the previously collected calibration points. If the deviation is sufficient, the mean value of the current measurement interval can be added to the set of calibration points.

In actigraphic measurements, stationary intervals are selected from human motion data during the collection of calibration points. Therefore, the duration of these motionless segments should be expressed in time independently of the sampling rate. Based on our experiments, we recommend the length of the stationary intervals to be at least 2-3 seconds, because too short intervals may lead to false steady state detections, and too long intervals may increase the time needed to collect enough calibration points. With these considerations in mind, we chose the length of stationary intervals to be 5 s, which also reduced the standard deviation of the noise to the tenth of resolution in our measurements.

For a microcontroller implementation, using the size of the flash memory page to determine the number of measurement points can be a good choice for segment length.

The detection of rest conditions is simply based on the difference between the maximum and minimum acceleration of one axis in one segment. In the case of worn actigraphs, it is enough to consider only one of the three axes since there is a low probability that a motion measured on one axis will not be present on the other two axes. The max-min value can be monitored during measurement, and at the end of the segment, it can be used to check if it is below a given threshold and if the current interval is stationary or not. Based on our experiments, $0.12\,g$ is a good choice for the max-min threshold level. The detection of the stationary segments is shown in Figure 4.
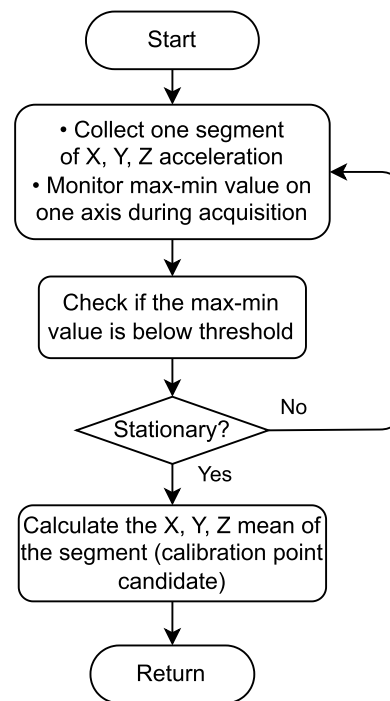

FIGURE 4. Detection of stationary intervals.

During measurement, the sum of the acceleration for each axis can be accumulated to provide the mean value at the end of the current segment (after dividing by the number of points). The mean value can then be tested to determine if it differs sufficiently from the already acquired calibration points.

This filtering is necessary because a significant portion of the mean values from rest intervals cluster around a few orientations which correspond to typical body postures (lying down, sitting, etc). This problem is visualized in Figure 5.

In our implementation, the selection of the rest intervals is achieved by splitting each X, Y, and Z axis into three intervals: $[-1.25\,g, -0.75\,g]$, $[-0.25\,g, 0.25\,g]$, $[0.75\,g, 1.25\,g]$. This partition groups the set of calibration points C into nine C_{ij} subsets, where $i \in x, y, z$ and $j \in n, 0, p$ (n: negative, 0: close
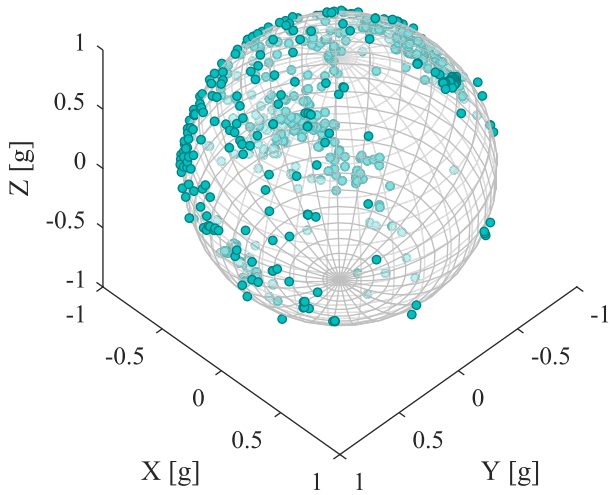
FIGURE 5. 2% of detected steady points acquired from the accelerometer data of a two-week-long wrist-worn actigraphic measurement. The distribution of the points is not even, as there are resting positions of the wrist that are more likely than others.

FIGURE 6. Testing whether the mean of the current segment can be saved as a calibration point.

to zero, p: positive):

$$C = \begin{bmatrix} C_{xn} & C_{yn} & C_{zn} \\ C_{x0} & C_{y0} & C_{z0} \\ C_{xp} & C_{yp} & C_{zp} \end{bmatrix}. \tag{10}$$

For each C_{ij} subset, the minimum and maximum number of points contained can be specified. We set both the minimum and maximum to 2, resulting in 18 calibration points. We examined how calibration accuracy depends on the number of calibration points in both simulations and on real raw acceleration data. Increasing the number from the minimum of 9 to 18 significantly improved accuracy. Increasing the number of points beyond 18 did not improve the accuracy. It is also noteworthy that increasing the number of calibration points also impacts the running time of the algorithm; however, we found that 18 points is an optimal compromise between accuracy and running time.

The algorithm to determine if the current point is needed is shown in Figure 6.

If the minimum number of calibration points is collected for each of the nine subsets, the iterative estimation of the error parameters can be initiated. An example of a suitable set of calibration points is shown in Figure 5.

To test the calibration on real, raw actigraphic data, we conducted 42 different activity measurements using 12 actigraphs. All 12 devices share the same specifications: 4.1 cm in length and a width of 1.6 cm, encapsulated in a plastic shell and worn on the wrist. The central component is a C8051F410 8-bit microcontroller that acquires acceleration data from an LIS3HD accelerometer and stores the raw data in a 1 Gb flash memory. A detailed description of the device can be found in [10].

We determined that two to three days of wrist-worn accelerometer data provided a satisfactory number of varied points for successful calibrations. The calibrated
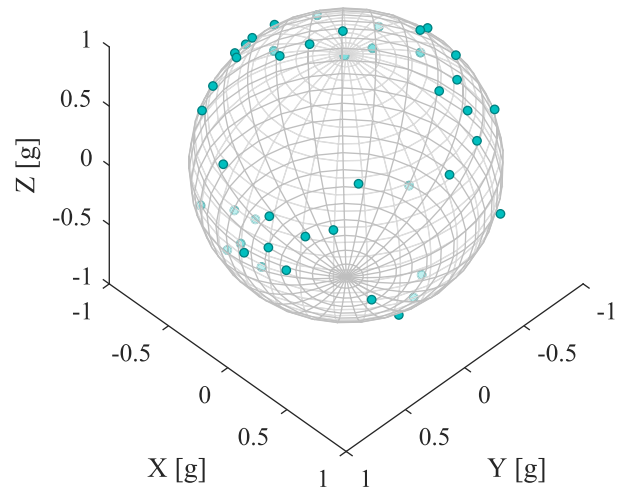
FIGURE 7. The selected three-dimensional calibration points from a wrist-worn actigraph. The selection method addresses the problem of the uneven distribution of resting points seen in Figure 5.

recordings are accessible on the internet via the following DOI: 10.6084/m9.figshare.16437684. The calibration process employed a method similar in principle to the one described here but utilized the global-search algorithm of LabVIEW. This dataset has been referenced in several of our works, including [10], [32], and [33].

The study was carried out as a part of research entitled "Examination neurobiological, cognitive and neurophenomenological aspects of the susceptibilities to mood swings or unusual experiences of healthy volunteer students,,, and was approved by the Human Investigation Review Board,

University of Szeged, Albert Szent-Györgyi Clinical Centre, Hungary (No 267/2018-SZTE) following its recommendations. All subjects gave written informed consent and the study was followed under the Declaration of Helsinki. All subjects were informed of their right to withdraw at any time without explanation and they were financially compensated.

C. OPTIMIZATION METHOD

The magnitude of acceleration measured by an ideal, motionless triaxial accelerometer is the local gravitational acceleration:

$$1\,\mathrm{g} = \sqrt{a_x^2 + a_y^2 + a_z^2}. \tag{11}$$

Measuring this value with an uncalibrated accelerometer will result in magnitudes that are different from 1 g and also depend on the orientation of the sensor. The more accurately the calibration coefficients are estimated, the smaller the deviation from 1 g will be after the correction, making this difference suitable as an objective function during the search for calibration coefficients. Adjusting a calibration point with the currently estimated calibration coefficients and subtracting 1 g can reveal the accuracy of the current estimation for one specific orientation. Calculating this value for each calibration point and summing the results gives a good metric for the goodness of the current calibration coefficients for all orientations, assuming that these points are as diverse as possible. Formally, the objective function is described as follows:

$$f(\boldsymbol{p}_n) = \sum_{i=1}^{N} \left(\sqrt{\hat{a}_x^2 + \hat{a}_y^2 + \hat{a}_z^2} - 1\,\mathrm{g} \right)^2, \tag{12}$$

where $\hat{a}_x$, $\hat{a}_y$, and $\hat{a}_z$ represent the measured acceleration values corrected by the n-th estimation of the calibration coefficients, $\boldsymbol{p}_n$, using formulas 7, 8, and 9, respectively. In low-power implementations, the computationally costly square root operation can be omitted since it does not affect the location of the cost function's minimum.

The presented method iteratively changes the calibration parameters to approach the local minimum of the objective function. The parameter vector that results from the last iteration is the one that best approximates the local minimum of the objective function and represents the final result of the calibration algorithm.

The initial values of the parameters are $\boldsymbol{p}_0 = \begin{bmatrix} 1\ 1\ 1\ 0\ 0\ 0\ 0\ 0\ 0 \end{bmatrix}^T$, which correspond to an ideal accelerometer. The algorithm changes one of the nine parameters by h and passes this slightly changed new parameter vector to the objective function. Performing this operation on all nine parameters, a vector whose i-th element is $f(\boldsymbol{p}_n^i)$, the value of the objective function for the parameter $\boldsymbol{p}_n^i$ incremented by h is obtained. By subtracting the result of the previous iteration, $\boldsymbol{p}_n$, and dividing by the step size h, an approximation of the gradient of the objective function,

$\nabla f(\boldsymbol{p}_n) \approx \boldsymbol{g}_n = \begin{bmatrix} g_{n1}, \dots, g_{n9} \end{bmatrix}$, is obtained:

$$g_{ni} = \frac{f(\boldsymbol{p}_n^i) - f(\boldsymbol{p}_n)}{h}. \tag{13}$$

In order to move towards the minimum, the calibration parameters need to be shifted in the direction of the negative gradient. This is achieved by subtracting the estimated gradient vector, weighted by the learning rate α, from the parameters. The new, n-th approximation of the calibration parameters is the result of this operation:

$$\boldsymbol{p}_{n+1} = \boldsymbol{p}_n - \alpha \boldsymbol{g}_n, \tag{14}$$

where $i = 1, \dots, 9$, the j-th element of $\boldsymbol{p}_n^i$ is

$$p_{n,j}^i = \begin{cases} p_{n,j}, & \text{if } j \neq i \\ p_{n,j} + h, & \text{if } j = i, \end{cases} \tag{15}$$

$j = 1, \dots, 9$ and h is the finite spacing for estimating the gradient.

The best choice of h depends on the number representation and the shape of f. If it is too small, it can lead to unacceptable truncation errors; if it is too big, it causes unacceptable formula errors. According to our simulation results, 10^{-5} is a good choice for double and single precision floating-point and 32-bit fixed-point implementations and 0.01 for the 16-bit fixed-point version.

The convergence of the misalignment parameters was found to be slower compared to the scale and offset parameters. The speed can be improved by replacing the scalar learning rate α with a vectorized learning rate.

$$\boldsymbol{\alpha} = \begin{bmatrix} \alpha_s \\ \alpha_s \\ \alpha_s \\ \alpha_m \\ \alpha_m \\ \alpha_m \\ \alpha_o \\ \alpha_o \\ \alpha_o \end{bmatrix}, \tag{16}$$

where α_s, α_m, α_o are different learning rates for scale, misalignment, and offset. A good set of learning rates was found to be $\alpha_s = 0.3$, $\alpha_m = 0.8$, $\alpha_o = 0.2$ when the square root was omitted. Regarding Figure 9, the calibration result converges after 20 to 30 iterations.

The algorithm involves performing $M \cdot (N \cdot 100 + 3)$ addition/subtraction operations and an equal number of multiplications. Here, M represents the number of iterations, and N is the total number of calibration points. As mentioned earlier, the implementation of this algorithm can completely avoid the use of floating-point calculations including the square root operation. This can drastically improve the overall running time even if the microcontroller has a hardware floating-point unit. We implemented simple test cases to test the cost of addition and multiplication on different architectures and different arithmetics. The results are shown in Table 1. We also measured the cost of the square root
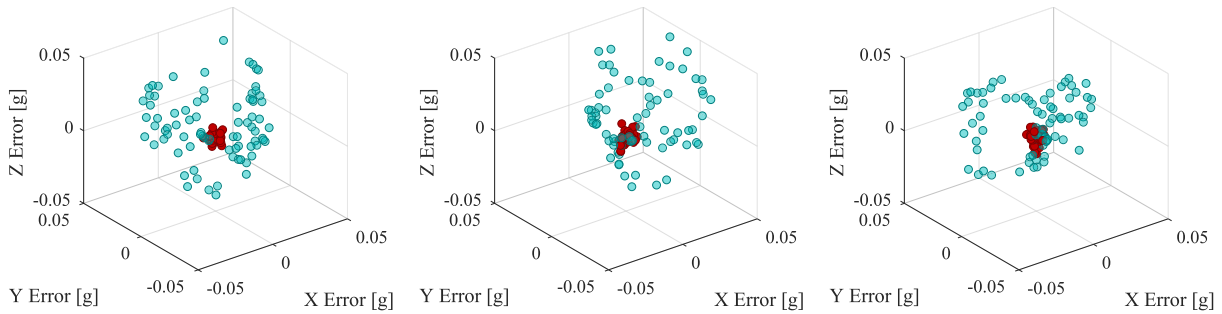
FIGURE 8. Three-dimensional stationary points before and after calibration. The magnitude values are reduced by 1 g to highlight the difference between the unit sphere and the measured values. The further a point is from the origin, the larger the difference compared to the expected ideal values. The cyan points correspond to uncalibrated stationary points, while the red ones represent the stationary points after applying the estimated coefficients to the uncalibrated cyan points.

operation, which required 2000 and 1711 clock cycles on the ARM Cortex-M3 and Cortex-M4 implementations, respectively.

If $M = 50$ and $N = 18$, as recommended, the integer operations take around 0.7 seconds on an ATmega328 8-bit microcontroller at 16 MHz and less than 40 ms on an ARM-Cortex M3 core clocked at 80 MHz. The floating-point implementation also executes under 30 ms on an ARM Cortex-M4 core at 80 MHz. While executing these operations, the current consumption of ATmega328 and ARM Cortex-M4 is typically 9.2 mA and 8.45 mA, respectively. Since the calibration is performed rarely (e.g., once every few days), running the optimization results in negligible additional power consumption of the continuous acceleration data acquisition. These characteristics demonstrate the feasibility of our method for ultra-low-power, coin cell or low-capacity battery-operated devices like actigraphs.

TABLE 1. Comparison of the cost of floating-point and integer arithmetic on different architectures, measured in clock cycles. The table presents data for three microcontroller units: the ATmega328, an 8-bit microcontroller; the ARM Cortex-M3, a 32-bit MCU core without a floating-point unit (FPU); and the ARM Cortex-M4, a microcontroller core equipped with a hardware FPU.

Processor	Addition		Multiplication	
	Integer	Float	Integer	Float
ATmega328	28	123	97	160
ARM Cortex-M3	14	96	14	68
ARM Cortex-M4	7	11	6	11

III. PERFORMANCE EVALUATION

The quality, reliability, and efficiency of the algorithm were verified through simulation and metrics based on measurements obtained from human-worn actigraphs.

In the simulation, the deterministic errors of the artificial calibration points are predefined and easily compared with the estimated values obtained as a result of the calibration. This comparison is not possible with real measurements because there is no direct knowledge of the errors inherent to the sensor inside the package, and they may change over time. The only known fact for real measurements is

that the magnitude of acceleration measured at rest must be 1 g in all orientations, and the deviation from this can serve as a measure of the quality of the calibration. For both simulation and real-measurement-based performance testing, the maximum iterations were set to 50, and all other parameters or variables of the algorithm were set as described in the previous sections.

We compared our method with two other published approaches; one of these is a non-iterative technique presented by Gietzelt et al. [34] that calculates scale and offset errors. An excellent MATLAB implementation of this technique is provided by Ailton Luiz Dias Siqueira Junior [35]. The other method is also written in MATLAB and utilizes the *fminunc* nonlinear built-in solver [31]. The error model in this method is essentially the same as the model presented in this paper, and the collection and selection of calibration points are also similar; however, its reproduction is challenging.

In addition to these, we implemented a calibration method based on LabVIEW's built-in global optimization procedure, which uses a differential evolution algorithm. We used our method to collect and select the calibration points for each of the compared calibration algorithms. Both MATLAB and LabVIEW are internationally recognized well-established, and widely used software packages. There is no doubt about the efficiency of their built-in optimization procedures.

A. SIMULATION

In the simulation-based verification, our aim was to replicate the calibration method described in [28]. We generated ideal points with unity magnitudes randomly to create artificial calibration points. These points were then modified by scale, misalignment, and offset errors, which were predetermined and formed a specific, pre-generated p parameter vector. Additionally, noise with standard deviations of 1 mg and 5 mg was added to the modified points. The described calibration point selection algorithm and the optimization were then performed on the generated points.

The artificial parameters were generated in the following ranges from uniform distribution with random
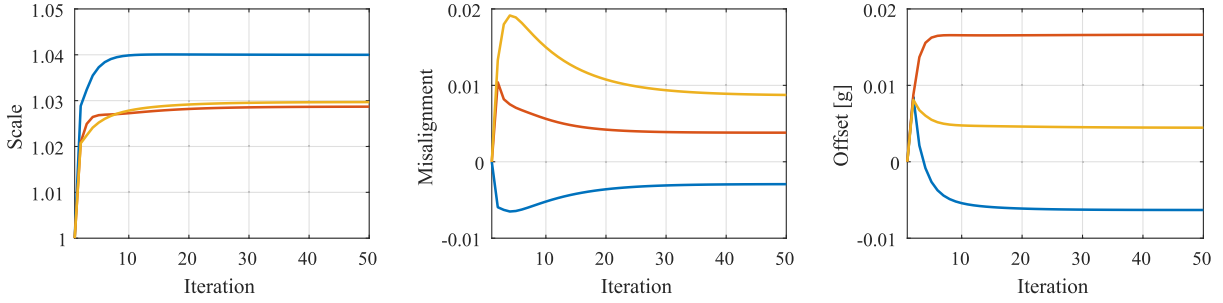
FIGURE 9. Convergence of the nine calibration parameters (x-axis in blue, y in red and z in yellow).

TABLE 2. Simulation results: the mean of the absolute differences between the generated and the estimated parameters. The simulation was run for 500 different scenarios with 1 mg and 5 mg added noise.

Parameter	Abs. Error Mean		Abs. Error SD	
	1 mg noise	5 mg noise	1 mg noise	5 mg noise
k_{xx}	$2.98 \cdot 10^{-4}$	$1.39 \cdot 10^{-3}$	$2.37 \cdot 10^{-4}$	$1.07 \cdot 10^{-3}$
k_{yy}	$3.18 \cdot 10^{-4}$	$1.64 \cdot 10^{-3}$	$2.27 \cdot 10^{-4}$	$1.22 \cdot 10^{-3}$
k_{zz}	$2.47 \cdot 10^{-4}$	$1.07 \cdot 10^{-3}$	$1.68 \cdot 10^{-4}$	$8.98 \cdot 10^{-4}$
k_{xy}	$1.49 \cdot 10^{-3}$	$2.61 \cdot 10^{-3}$	$1.22 \cdot 10^{-3}$	$2.24 \cdot 10^{-3}$
k_{xz}	$1.42 \cdot 10^{-3}$	$2.67 \cdot 10^{-3}$	$1.23 \cdot 10^{-3}$	$2.07 \cdot 10^{-3}$
k_{yz}	$1.45 \cdot 10^{-3}$	$3.3 \cdot 10^{-3}$	$1.26 \cdot 10^{-3}$	$2.53 \cdot 10^{-3}$
o_x [g]	$2.39 \cdot 10^{-4}$	$1.05 \cdot 10^{-3}$	$1.88 \cdot 10^{-4}$	$9.2 \cdot 10^{-4}$
o_y [g]	$2.54 \cdot 10^{-4}$	$1.18 \cdot 10^{-3}$	$1.91 \cdot 10^{-4}$	$8.35 \cdot 10^{-4}$
o_z [g]	$2.04 \cdot 10^{-4}$	$1.08 \cdot 10^{-3}$	$1.5 \cdot 10^{-4}$	$7.76 \cdot 10^{-4}$

generator: scale: $(0.9, 1.1)$, misalignment: $(-0.05, 0.05)$, offset: $(-0.1\,\text{g}, 0.1\,\text{g})$:

$$S_i = 2 \cdot \left(\delta - \frac{1}{2}\right) \cdot 0.1 + 1,$$

$$T_j = 2 \cdot \left(\delta - \frac{1}{2}\right) \cdot 0.05,$$

$$O_i = 2 \cdot \left(\delta - \frac{1}{2}\right) \cdot 0.1\,\text{g}, \tag{17}$$

where δ is a random floating-point number between 0 and 1, $i \in \{x, y, z\}$ and $j \in \{xy, xz, yz\}$. The elements of the simulated $\boldsymbol{p}$ are obtained as follows:

$$
\begin{aligned}
p_1 &= k_{xx} = S_x \\
p_2 &= k_{yy} = S_y \\
p_3 &= k_{zz} = S_z \\
p_4 &= k_{xy} = S_y \cdot T_{xy} \\
p_5 &= k_{xz} = S_z \cdot T_{xz} \\
p_6 &= k_{yz} = S_z \cdot T_{yz} \\
p_7 &= o_x \\
p_8 &= o_y \\
p_9 &= o_z
\end{aligned} \tag{18}
$$

The artificial calibration points are generated using the following equations (the inverse of applying

the calibration parameters):

$$c_{ix} = \frac{a_x}{k_{xx}} - o_x$$

$$c_{iy} = \frac{a_y - (c_{ix} - o_x)\, k_{xy}}{k_{yy}} - o_y$$

$$c_{iz} = \frac{a_z - (c_{ix} + o_x)\, k_{xz} - (c_{iy} + o_y)\, k_{yz}}{k_{zz}} - o_z, \tag{19}$$

$$u_{ij} = c_{ij} + \epsilon_{ij}, \, (i = 1, \ldots, N), \, (j = x, y, z), \tag{20}$$

where (a_{ix}, a_{iy}, a_{iz}) is the i-th randomly generated calibration point with a unit magnitude, (c_{ix}, c_{iy}, c_{iz}) is the i-th simulated steady point without added noise, ϵ is a random floating-point number from normal distribution with standard deviation of $\pm 1\,\text{mg}$ and $\pm 5\,\text{mg}$ and (u_{ix}, u_{iy}, u_{iz}) is simulated steady point with added noise.

The simulation was run for 500 different cases, and the mean absolute error of the estimated values, as well as their standard deviations, were calculated (see Table 2). Ideally, the result of the calibration should be equal to the pre-generated values. The difference reveals how precisely can the algorithm estimate $\boldsymbol{p}$.

B. TESTS AND METRICS BASED ON REAL ACTIGRAPH DATA

The accuracy of the calibration was also evaluated using 5-10 days of real acceleration data. Two distinct sets of calibration points were collected for each dataset: the first set was used for calibration, while the second set served as

TABLE 3. The average of the absolute differences between the measured magnitudes and $1\,\mathrm{g}$ in motionless intervals before and after the calibration. The set of motionless intervals is distinct from the set used for the calibration.

Method	$\lvert r - 1 \rvert$ [mg] (Before Calibraion)	$\lvert \hat{r} - 1 \rvert$ [mg] (After Calibraiton)	Improvement
Our method	25.1	3.06	820%
Non-iterative method	25.1	4.08	615%
MATLAB *fminunc*	25.1	3.16	794%
LabVIEW global	25.1	3.27	768%

control points for metric calculation. Before (r) and after ($\hat{r}$) calibration, the mean magnitude of the control points was determined. Ideally, subtracting the local gravity should yield zero. By taking the absolute values and comparing $\lvert r - 1 \rvert$ with $\lvert \hat{r} - 1 \rvert$, we can assess the accuracy before and after calibration. The relative improvement in accuracy enables easy comparison among different calibration methods:

$$R = \left| \frac{r - 1}{\hat{r} - 1} \right| \cdot 100\%. \quad (21)$$

The experiments were performed on ten different datasets, each measured using a different actigraph device. All four methods significantly improved the accuracy of the accelerometers. Based on the findings presented in the Table 3, it can be concluded that the proposed method achieves the same level of accuracy to the built-in global optimization algorithms of LabVIEW and MATLAB.

IV. SUMMARY

This article introduces a straightforward and efficient algorithm for calibrating triaxial accelerometers. The algorithm is designed to be implemented on microcontrollers with limited computational capabilities, making it suitable for use in small, battery-powered devices like actigraphs. It offers the flexibility to calibrate accelerometers in real-time while they are being worn or to calibrate pre-collected data. The algorithm has been thoroughly tested using both simulated and real human-worn accelerometer data. The results demonstrate that the calibration performance of the proposed method is practically the same as that of established global optimization algorithms found in MATLAB and LabVIEW; however, the computation cost is much lower. Our results suggest that more complex global-search algorithms do not significantly enhance the calibration and its performance compared to a simple local search presented in this paper. The method is not only suitable for calibrating actigraphs but can also be used in any mobile IoT smart device.

REFERENCES

[1] D. H. Titterton and J. L. Weston, *Strapdown Inertial Navigation Technology* (IEE Radar, Sonar, Navigation, and Avionics Series), 2nd ed. Stevenage, U.K.: Institution of Electrical Engineers, 2004.

[2] S. Garrigue, C. Gentilini, F. Hofgartner, E. Mouton, A. Rousseau, and J. Clementy, "Performance of a rate responsive accelerometer-based pacemaker with autocalibration during standardized exercise and recovery," *Pacing Clin. Electrophysiol.*, vol. 25, no. 6, pp. 883–887, Jun. 2002, doi: 10.1046/j.1460-9592.2002.t01-1-00883.x.

[3] K. J. Rebello, "Applications of MEMS in surgery," *Proc. IEEE*, vol. 92, no. 1, pp. 43–55, Jan. 2004. [Online]. Available: http://ieeexplore.ieee.org/document/1258171/

[4] D. M. González-Otero, J. M. Ruiz, S. R. de Gauna, J. J. Gutiérrez, M. Daya, J. K. Russell, I. Azcarate, and M. Leturiondo, "Monitoring chest compression quality during cardiopulmonary resuscitation: Proof-of-concept of a single accelerometer-based feedback algorithm," *PLoS ONE*, vol. 13, no. 2, Feb. 2018, Art. no. e0192810.

[5] K. L. Dominik, "Long-term activity and movement monitoring in neurological patients," Ph.D. dissertation, Dept. Health Sci. Technol., ETH Zurich, Zurich, Switzerland, 2015, p. 198. [Online]. Available: http://hdl.handle.net/20.500.11850/122013

[6] D. Fekedulegn, M. E. Andrew, M. Shi, J. M. Violanti, S. Knox, and K. E. Innes, "Actigraphy-based assessment of sleep parameters," *Ann. Work Exposures Health*, vol. 64, no. 4, pp. 350–367, Apr. 2020. [Online]. Available: https://academic.oup.com/annweh/article/64/4/350/5735350

[7] R. S. Falck, G. J. Landry, K. Brazendale, and T. Liu-Ambrose, "Measuring physical activity in older adults using MotionWatch 8 actigraphy: How many days are needed?" *J. Aging Phys. Activity*, vol. 25, no. 1, pp. 51–57, Jan. 2017. [Online]. Available: http://journals.humankinetics.com/doi/10.1123/japa.2015-0256

[8] N. Gravett, A. Bhagwandin, R. Sutcliffe, K. Landen, M. J. Chase, O. I. Lyamin, J. M. Siegel, and P. R. Manger, "Inactivity/sleep in two wild free-roaming African elephant matriarchs—Does large body size make elephants the shortest mammalian sleepers?" *PLoS ONE*, vol. 12, no. 3, Mar. 2017, Art. no. e0171903.

[9] L. G. Adlan, M. Csordás-Nagy, B. Bodosi, G. Kalmár, L. G. Nyúl, A. Nagy, G. Kekesi, A. Büki, and G. Horvath, "Sleep-wake rhythm and oscillatory pattern analysis in a multiple hit schizophrenia rat model (Wisket)," *Frontiers Behav. Neurosci.*, vol. 15, Jan. 2022, Art. no. 799271. [Online]. Available: https://www.frontiersin.org/articles/10.3389/fnbeh.2021.799271/full

[10] B. Maczák, G. Vadai, A. Dér, I. Szendi, and Z. Gingl, "Detailed analysis and comparison of different activity metrics," *PLoS ONE*, vol. 16, no. 12, Dec. 2021, Art. no. e0261718, doi: 10.1371/journal.pone.0261718.

[11] *MEMS Digital Output Motion Sensor: Ultra-Low-Power High-Performance 3-Axis 'Nano' Accelerometer*, STMicroelectronics, Geneva, Switzerland, p. 55, 2016.

[12] *iNEMO Inertial Module: Always-on 3D Accelerometer and 3D Gyroscope*, STMicroelectronics, Geneva, Switzerland, p. 115, 2017.

[13] H.-P. Trah, J. Franz, and J. Marek, "Physics of semiconductor sensors," in *Advances in Solid State Physics*, vol. 39, B. Kramer, Ed. Berlin, Germany: Springer, 1999, pp. 25–36. [Online]. Available: http://link.springer.com/10.1007/BFb0107462

[14] P. Batista, C. Silvestre, P. Oliveira, and B. Cardeira, "Accelerometer calibration and dynamic bias and gravity estimation: Analysis, design, and experimental evaluation," *IEEE Trans. Control Syst. Technol.*, vol. 19, no. 5, pp. 1128–1137, Sep. 2011. [Online]. Available: http://ieeexplore.ieee.org/document/5594974/

[15] Z. C. Wu, Z. F. Wang, and Y. Ge, "Gravity based online calibration for monolithic triaxial accelerometers' gain and offset drift," in *Proc. 4th World Congr. Intell. Control Autom.* Shanghai, China: IEEE, 2002, pp. 2171–2175. [Online]. Available: http://ieeexplore.ieee.org/document/1021471/

[16] M. El-Diasty, A. El-Rabbany, and S. Pagiatakis, "Temperature variation effects on stochastic characteristics for low-cost MEMS-based inertial sensor error," *Meas. Sci. Technol.*, vol. 18, no. 11, pp. 3321–3328, Nov. 2007.

[17] E. Renk, M. Rizzo, W. Collins, F. Lee, and D. Bernstein, "Calibrating a triaxial accelerometer-magnetometer—Using robotic actuation for sensor reorientation during data collection," *IEEE Control Syst. Mag.*, vol. 25, no. 6, pp. 86–95, Dec. 2005.

[18] J. Pan, C. Zhang, and Q. Cai, "An accurate calibration method for accelerometer nonlinear scale factor on a low-cost three-axis turntable," *Meas. Sci. Technol.*, vol. 25, no. 2, Feb. 2014, Art. no. 025102. [Online]. Available: https://iopscience.iop.org/article/10.1088/0957-0233/25/2/025102

[19] R. Zhang, F. Hoflinger, and L. M. Reind, "Calibration of an IMU using 3-D rotation platform," *IEEE Sensors J.*, vol. 14, no. 6, pp. 1778–1787, Jun. 2014.

[20] E. L. Renk, W. Collins, M. Rizzo, F. Lee, and D. S. Bernstein, "Optimization-based calibration of a triaxial accelerometer-magnetometer," in *Proc., Amer. Control Conf.* Portland, OR, USA: IEEE, Jun. 2005, pp. 1957–1962. [Online]. Available: http://ieeexplore.ieee.org/document/1470256/

[21] Q. Cai, N. Song, G. Yang, and Y. Liu, "Accelerometer calibration with nonlinear scale factor based on multi-position observation," *Meas. Sci. Technol.*, vol. 24, no. 10, Oct. 2013, Art. no. 105002. [Online]. Available: https://iopscience.iop.org/article/10.1088/0957-0233/24/10/105002

[22] *Parameters Calibration a Low-G 3-Axis Accelerometer*, STMicroelectronics, Geneva, Switzerland, 2014.

[23] A. Krohn, M. Beigl, C. Decker, U. Kochendörfer, P. Robinson, and T. Zimmer, "Inexpensive and automatic calibration for acceleration sensors," in *Ubiquitous Computing Systems*, vol. 3598, D. Hutchison, T. Kanade, J. Kittler, J. M. Kleinberg, F. Mattern, J. C. Mitchell, M. Naor, O. Nierstrasz, C. P. Rangan, B. Steffen, M. Sudan, D. Terzopoulos, D. Tygar, M. Y. Vardi, G. Weikum, H. Murakami, H. Nakashima, H. Tokuda, and M. Yasumura, Eds. Berlin, Germany: Springer, 2005, pp. 245–258. [Online]. Available: https://link.springer.com/10.1007/11526858

[24] M. Glueck, D. Oshinubi, P. Schopp, and Y. Manoli, "Real-time autocalibration of MEMS accelerometers," *IEEE Trans. Instrum. Meas.*, vol. 63, no. 1, pp. 96–105, Jan. 2014. [Online]. Available: http://ieeexplore.ieee.org/document/6579769/

[25] H. Zhang, Y. Wu, W. Wu, M. Wu, and X. Hu, "Improved multi-position calibration for inertial measurement units," *Meas. Sci. Technol.*, vol. 21, no. 1, Jan. 2010, Art. no. 015107. [Online]. Available: https://iopscience.iop.org/article/10.1088/0957-0233/21/1/015107

[26] I. Frosio, F. Pedersini, and N. A. Borghese, "Autocalibration of MEMS accelerometers," *IEEE Trans. Instrum. Meas.*, vol. 58, no. 6, pp. 2034–2041, Jun. 2009. [Online]. Available: http://ieeexplore.ieee.org/document/4655611/

[27] F. Camps, S. Harasse, and A. Monin, "Numerical calibration for 3-axis accelerometers and magnetometers," in *Proc. IEEE Int. Conf. Electro/Information Technol.* Windsor, ON, Canada: IEEE, Jun. 2009, pp. 217–221. [Online]. Available: https://ieeexplore.ieee.org/document/5189614/

[28] L. Ye, A. Argha, B. G. Celler, H. T. Nguyen, and S. W. Su, "Online auto-calibration of triaxial accelerometer with time-variant model structures," *Sens. Actuators A, Phys.*, vol. 266, pp. 294–307, Oct. 2017. [Online]. Available: https://linkinghub.elsevier.com/retrieve/pii/S0924424717308634

[29] S. Bonnet, C. Bassompierre, C. Godin, S. Lesecq, and A. Barraud, "Calibration methods for inertial and magnetic sensors," *Sens. Actuators A, Phys.*, vol. 156, no. 2, pp. 302–311, Dec. 2009. [Online]. Available: https://linkinghub.elsevier.com/retrieve/pii/S0924424709004324

[30] L. Ye and S. W. Su, "Optimum experimental design applied to MEMS accelerometer calibration for 9-parameter auto-calibration model," in *Proc. 37th Annu. Int. Conf. IEEE Eng. Med. Biol. Soc. (EMBC)*, Aug. 2015, pp. 3145–3148. [Online]. Available: http://ieeexplore.ieee.org/document/7319059/

[31] J. Rohac, M. Sipos, and J. Simanek, "Calibration of low-cost triaxial inertial sensors," *IEEE Instrum. Meas. Mag.*, vol. 18, no. 6, pp. 32–38, Dec. 2015. [Online]. Available: http://ieeexplore.ieee.org/document/7335836/

[32] Á. Nagy, J. Dombi, M. P. Fülep, E. Rudics, E. A. Hompoth, Z. Szabó, A. Dér, A. Búzás, Z. J. Viharos, A. T. Hoang, B. Maczák, G. Vadai, Z. Gingl, S. László, V. Bilicki, and I. Szendi, "The actigraphy-based identification of premorbid latent liability of schizophrenia and bipolar disorder," *Sensors*, vol. 23, no. 2, p. 958, Jan. 2023. [Online]. Available: https://www.mdpi.com/1424-8220/23/2/958

[33] B. Maczák, Z. Gingl, and G. Vadai, "General spectral characteristics of human activity and its inherent scale-free fluctuations," *Sci. Rep.*, vol. 14, no. 1, p. 2604, Jan. 2024. [Online]. Available: https://www.nature.com/articles/s41598-024-52905-8

[34] M. Gietzelt, K.-H. Wolf, M. Marschollek, and R. Haux, "Performance comparison of accelerometer calibration algorithms based on 3D-ellipsoid fitting methods," *Comput. Methods Programs Biomed.*, vol. 111, no. 1, pp. 62–71, Jul. 2013. [Online]. Available: https://linkinghub.elsevier.com/retrieve/pii/S0169260713000825

[35] A. L. D. Siqueira Jr. *MATLAB Accelerometer Calibration Functions*. Accessed: Jun. 29, 2023. [Online]. Available: https://github.com/ailtonljr/AccelerometerCalibration

DENES FARAGO received the B.S. and M.S. degrees in computer science engineering from the University of Szeged, Hungary. He has been contributing to university teaching, since 2017. He started his full-time occupation as a Junior Assistant Professor with the Department of Technical Informatics, in 2022. His research interests include analog electronics, signal processing, atomic force microscopy, and the application of embedded systems in multidisciplinary sciences in general.

BALINT MACZAK received the B.S. and M.S. degrees in computer science engineering from the University of Szeged, Hungary. He is currently pursuing the Ph.D. degree in human actigraphy and activity analysis (computer science). He has been contributing to university teaching and research and development projects, since 2016 and 2018, respectively.

ZOLTAN GINGL received the M.Sc. and Ph.D. degrees in physics from the University of Szeged, Hungary, and the D.Sc. degree in electrical engineering from the Hungarian Academy of Sciences. Since 1989, he has been with the University of Szeged, where he is currently a Full Professor and the Head of the Department of Technical Informatics. He has published numerous articles related to various fields, including noise and fluctuations, secure communications, and multidisciplinary software-defined instrumentation and education.